

## ARTICLE OPEN



# Intrinsically stretchable light-emitting drawing displays

Jiaxue Zhang<sup>1,2,3</sup>, Qianying Lu<sup>1,2,3</sup>, Ming Wu<sup>4</sup>, Yuping Sun<sup>1,2,3</sup>, Shaolei Wang<sup>1,2,3</sup>, Xiaoliang Wang<sup>4</sup>✉, Ming-Hui Lu<sup>1,2</sup>✉ and Desheng Kong<sup>1,2,3</sup>✉

Stretchable displays that combine light-emitting capabilities with mechanical compliance are essential building blocks of next-generation wearable electronics. However, their widespread applications are currently limited by complex device architecture, limited pixel density, and immature fabrication processes. In this study, we present the device design and material developments of intrinsically stretchable light-emitting drawing displays that can show arbitrary hand-drawing features. The alternating-current electroluminescent display uses a simplified architecture comprising coplanar interdigitated liquid metal electrodes, an electroluminescent layer, and a dielectric encapsulation layer. Ink patterns on the device are coupled with the interdigitated electrodes under alternating voltage stimulations, generating localized electric fields for bright emissions. Various inks are prepared for painting, stamping, and stencil printing. Arbitrary luminous features on the devices can be either long-lasting or transient in characteristics. These skin-like devices are made entirely of compliant materials that can withstand bending, twisting, and stretching manipulations. Due to the excellent mechanical deformability, the drawing displays can be conformally laminated on the skin as body-integrated optoelectronic communication devices for graphic information.

*npj Flexible Electronics* (2024)8:1 | <https://doi.org/10.1038/s41528-023-00287-8>

## INTRODUCTION

Stretchable electronics can be a game changer for next-generation wearables. Conformal integration with the human body is made possible through the stable operation of skin-like devices under bent, twisted, and stretched conditions<sup>1–7</sup>. Soft and deformable light-emitting devices are particularly appealing for emerging applications, such as skin-like lighting<sup>8</sup>, wearable sensors<sup>9–11</sup>, soft robotics<sup>12,13</sup>, and fashion designs<sup>14,15</sup>. There are two main design strategies for stretchable light-emitting devices. A straightforward strain engineering approach develops extensible configurations based on conventional optoelectronic materials, including origami/kirigami architectures<sup>16,17</sup>, interconnected island-bridge structures<sup>18,19</sup>, and wrinkled surfaces<sup>20–22</sup>. However, these mechanically structured devices often sacrifice visual effects and skin-like deformability. Another approach exploits all compliant materials to construct various intrinsically stretchable devices, such as organic/perovskite light-emitting diodes<sup>23–25</sup>, light-emitting electrochemical cells<sup>26,27</sup>, and alternating-current electroluminescent (AC EL) devices<sup>12,28,29</sup>. In particular, the stretchable AC EL device commonly has an emission composite sandwiched between two planar electrodes. In the composite layer, the phosphor microparticles are dispersed in a dielectric elastomer matrix and are activated by alternating electric fields for light emissions<sup>30,31</sup>. The luminance patterns of these sandwiched AC EL devices are therefore defined by the overlapping areas of the top and bottom electrodes. Their simplified architecture and convenient assembly have already attracted intensive research attention recently<sup>32–34</sup>. Despite excellent mechanical deformability, intrinsically stretchable light-emitting devices often exhibit less competitive optoelectronic properties than traditional rigid devices. Interestingly, recent studies have shown promise of

emerging compliant electroluminescent materials to gradually close the performance gaps<sup>35,36</sup>.

Stretchable light-emitting devices can easily illuminate static patterns. To provide complex visual information, dynamically refreshable displays have also been developed comprising luminous pixels coupled with control circuits. Intuitively, individually addressable elements form the stretchable segmented display suitable for predetermined contents like numbers and characters. These devices are demonstrated in practical settings in terms of deformable counters<sup>37</sup>, skin-attachable clocks<sup>38</sup>, and interactive textiles<sup>39,40</sup>. Alternatively, the matrix display uses conductor grids to control each luminous pixel<sup>27</sup>. The simplified architecture facilitates the scalable fabrication of large-area displays for arbitrary graphic patterns. In addition, active-driven matrix displays have been recently demonstrated with stretchable thin-film transistors that improve the pattern refresh rates and pixel brightness<sup>41</sup>. In addition to monochromatic emissions, compliant multicolor displays are also developed by combining different emissive elements<sup>42,43</sup>. Despite the rapid progress, the pixel density of stretchable displays still needs to catch up with their rigid counterparts due to limited material performances and immature fabrication techniques. Creating high-performing displays in deformable form factors remains a practical challenge.

In this study, we present the design and fabrication of intrinsically stretchable light-emitting drawing displays. In a simplified architecture, the device utilizes the AC EL operating mechanism to achieve luminous features that resemble the ink patterns and allow convenient delivery of complex graphic information. The drawing display is made entirely of compliant components to achieve skin-like deformability, including interdigitated liquid metal electrodes, an electroluminescent layer, and a dielectric encapsulation layer. The ionically conductive ink is

<sup>1</sup>College of Engineering and Applied Sciences, National Laboratory of Solid State Microstructure, and Collaborative Innovation Center of Advanced Microstructures, Nanjing 210093, China. <sup>2</sup>Jiangsu Key Laboratory of Artificial Functional Materials, Nanjing University, Nanjing 210023, China. <sup>3</sup>State Key Laboratory of Analytical Chemistry for Life Science, Nanjing University, Nanjing 210023, China. <sup>4</sup>Key Laboratory of High Performance Polymer Materials and Technology of Ministry of Education, Department of Polymer Science and Engineering, School of Chemistry and Chemical Engineering, Nanjing University, Nanjing 210023, China. ✉email: wangxiaoliang@nju.edu.cn; luminghui@nju.edu.cn; dskong@nju.edu.cn

easily drawn into patterned top electrodes and capacitively coupled with interdigitated liquid metal electrodes to activate bright emissions. Different aqueous inks formulated with tailored rheological properties can create arbitrary patterns through painting, stamping, and stencil printing. The standard inks produce transient luminous patterns due to water evaporation, allowing for continuous drawing for real-time communications. On the other hand, ink patterns with hygroscopic salts are suitable for long-term display and can easily be erased for repetitive uses. The stretchable light-emitting drawing displays are robust enough to withstand up to 200% tensile strain and repetitive stretching. Conformally laminating them on the skin demonstrates their practical suitability as body-integrated displays for graphic information. The device design and material developments reported here may find a broad range of applications in stretchable and wearable optoelectronic systems.

## RESULTS AND DISCUSSIONS

### Design and fabrication of stretchable light-emitting displays

Figure 1a schematically illustrates the stretchable light-emitting drawing display that emits light from the painted patterns. The drawing displays in green, blue, and orange colors are achieved using different ZnS phosphors, as shown in Fig. 1b. In contrast to conventional sandwich architecture, the AC EL device is comprised of interdigitated liquid metal electrodes, a light-emitting layer, and a dielectric encapsulation layer, as shown in Fig. 1c. The liquid metal used here is an eutectic alloy of gallium, indium, and tin that features high electrical conductivity of  $3.46 \times 10^4 \text{ S cm}^{-1}$ , a low melting point below room temperature, and negligible toxicity<sup>44–46</sup>. The ionically conductive ink is an aqueous solution containing inorganic salt and polymer, which is drawn into a floating top electrode without direct connection to the electrical circuit. An alternating voltage on the interdigitated electrodes is capacitively coupled with the ink, activating the embedded ZnS phosphor microparticles for bright emissions<sup>47</sup>. Discrete luminous patterns are consequently generated on the device consistent with the drawing paths. In Fig. 1d, a representative device displays a hand-painted smiling-face pattern. The device exploits

compliant materials to achieve skin-like deformability, which is sufficiently robust to withstand bending, twisting, and stretching manipulations. In addition, the luminous pattern is easily cleaned through wiping or rinsing for repeated uses, as shown in Supplementary Video 1.

Figure 2a schematically reveals the fabrication process of the stretchable light-emitting drawing display. The liquid metal film is prepared using a method that has been reported previously<sup>48</sup>. Initially, a Cr/Cu film is thermally evaporated onto the elastomer substrate as the wetting layer. The liquid metal is cleaned with dilute acid and spread on the metalized substrate. The extra liquid metal is removed through high-rate rotation in a spin coater, producing a smooth and uniform film with a thickness of  $\sim 1.6 \mu\text{m}$ . Selective laser ablation allows subtractive patterning of the liquid metal film into interdigitated electrodes. A subsequent spin-casting step defines the light-emitting layer comprising a PVDF-HFP elastomer matrix, ZnS phosphor microparticles, and BaTiO<sub>3</sub> (BTO) nanoparticles. BTO nanoparticles are high-*k* ceramic fillers of the composite to boost its dielectric properties and emission intensity (see Supplementary Fig. 1). A thin PVDF-HFP layer is spin-cast over the entire substrate to prevent premature dielectric breakdown. Figure 2b reveals a representative liquid metal electrode in an interdigitated configuration comprising  $\sim 600 \mu\text{m}$  fingers and  $\sim 150 \mu\text{m}$  gaps. The smooth edges and uniform spacings demonstrate excellent patterning quality through selective laser ablation. The liquid metal electrodes exhibit high electrical conductivity, excellent stretchability, and optical reflectivity<sup>48</sup>. In Fig. 2c, a cross-sectional microscopy image of the device reveals the bilayer structure of the electroluminescent composite, consisting of a  $\sim 10 \mu\text{m}$ -thick light-emitting layer and a  $\sim 4 \mu\text{m}$ -thick PVDF-HFP dielectric layer. As-prepared devices display graphic patterns following the shape of the floating electrode. An aqueous ink dissolved with inorganic salts defines the floating electrode. A regular aqueous droplet exhibits a large contact angle of  $105^\circ$  on the dielectric encapsulation, as shown in Fig. 2d. A fluorinated surfactant is added to the ink formulation for an effectively reduced contact angle of  $54^\circ$ . The improved wettability facilitates the formation of continuous drawing patterns. In addition, the aqueous ink exhibits high optical transmittance

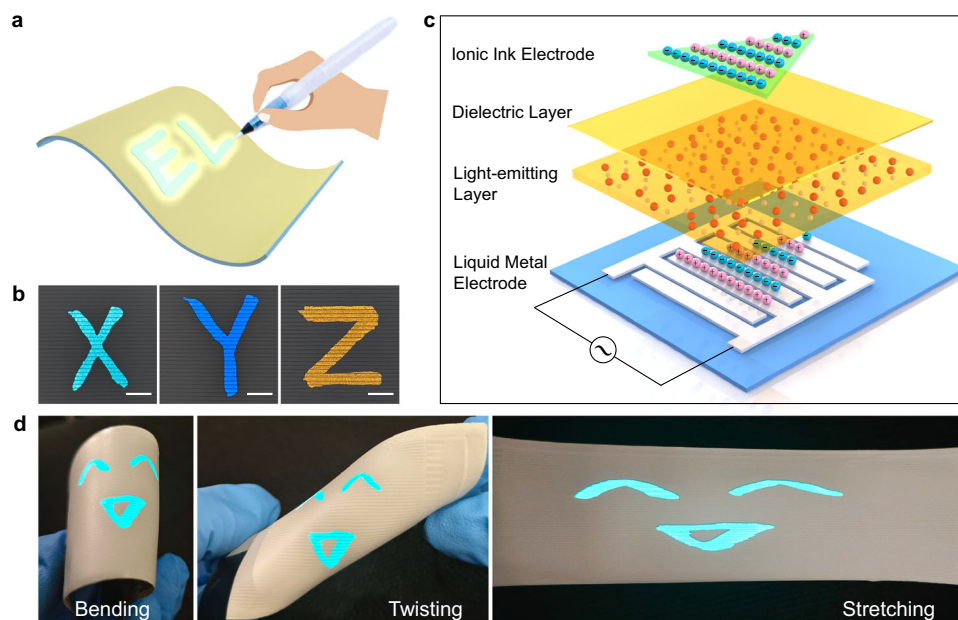


**Fig. 1** Stretchable light-emitting drawing displays. **a** Schematic illustrating the operation of light-emitting drawing displays. **b** As-prepared devices emitting light in green, blue, and orange, respectively. Scale bars: 0.5 mm. **c** Exploded view of the device architecture comprising liquid metal interdigitated electrodes, a light-emitting layer, a dielectric encapsulation layer, and an ionically conductive ink electrode. **d** Mechanical manipulation of a representative device with a smiling face luminous pattern by bending, twisting, and stretching.

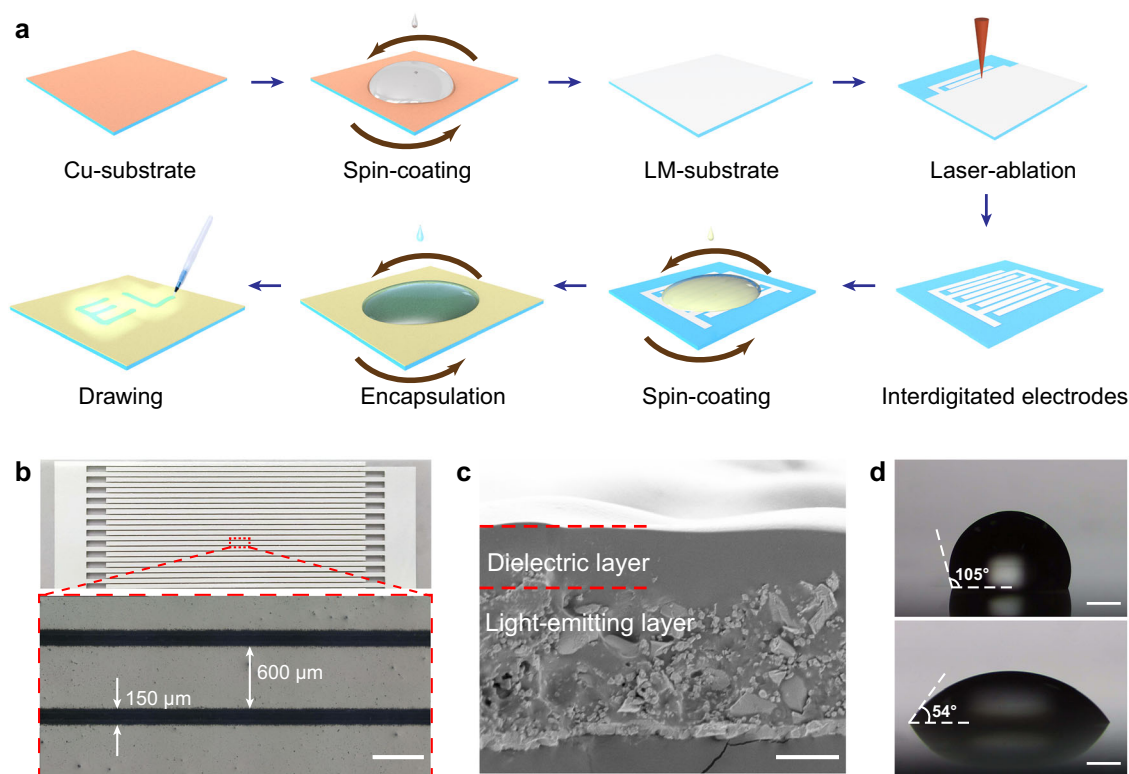


**Fig. 2 Fabrication process and material components.** **a** Schematic illustration of the step-by-step fabrication process. **b** Optical (top) and optical microscopy (bottom) images of liquid metal interdigitated electrodes. Scale bar: 500  $\mu\text{m}$ . **c** SEM image showing the device cross-section with the light-emitting and dielectric layers. Scale bar: 5  $\mu\text{m}$ . **d** Contact angle images of the pristine (top) and surfactant-incorporated aqueous droplets on PVDF-HFP elastomers. Scale bars: 500  $\mu\text{m}$ .

from visible to near infrared wavelengths, which is well suitable to prepare the top electrode for excellent light extraction (see Supplementary Fig. 2).

### Light-emitting mechanism and characteristics

The as-prepared light-emitting drawing display illuminates arbitrary and complex patterns from the overlapping area of the drawing ink and the interdigitated electrodes. Figure 3a presents a representative device displaying a hand-drawing landscape sketch. The corresponding optical microscopy image reveals stripe-like luminous patterns. Without the ink electrode, the applied voltage on the interdigitated electrodes is expected to create lateral electric fields. Here, the electric field distribution during an alternating voltage cycle has been modified with the drawing ink patterns, as shown in the schematic diagram in Fig. 3b. Anions and cations of the ionic conductor are collected above the positive and negative finger electrodes, leading to the formation of miniaturized capacitors<sup>47</sup>. The alternating voltages at adjacent finger electrodes (A and B) therefore generate vertical electric fields in opposite directions, activating the embedded phosphor microparticles for light emissions. Due to the voltage split between adjacent finger electrodes, the effective voltage amplitude on these miniaturized capacitors is approximately half of the applied alternating voltage, as shown in Fig. 3c. Figure 3d shows luminance *versus* applied voltage amplitude (20 kHz, square waveform) for a representative device that emits green light. Since our device is powered by alternating electric fields, the luminance follows the standard behavior of AC EL devices expressed using the equation  $L = L_0 \exp(-\beta/V^{1/2})$ , where  $L$  is the luminance,  $V$  is the voltage amplitude, and  $L_0$  and  $\beta$  are device-specific fitting parameters<sup>49</sup>. These drawing displays emit 11  $\text{cd m}^{-2}$  at 60 V and 46  $\text{cd m}^{-2}$  at 100 V when using deionized (DI) water-based ink. If a LiCl-based ink is utilized, these devices can emit 26  $\text{cd m}^{-2}$  at 60 V and 134  $\text{cd m}^{-2}$  at 100 V, making it the preferred

ink choice due to its abundant ions with improved polarizability. In addition, the emission of blue and orange drawing displays also increases with the applied voltage amplitudes (see Supplementary Fig. 3). However, the emission intensities are lower than that of the green one due to the strong influence of the dopants on ZnS emission bands and efficiencies<sup>50</sup>. In Fig. 3e, the emission intensity is also affected by modulating the voltage frequency. The initial rise with the frequency is attributed to the increased electron injections that activate the luminescent centers<sup>51,52</sup>. However, the luminance drops with further increased frequency due to injected electrons trapped at donor levels<sup>53,54</sup>. The peak emission intensity is therefore achieved at an intermediate frequency of  $\sim 20$  kHz. Additionally, the emission color has a blue shift by raising voltage frequencies, as depicted in Supplementary Fig. 4a. The combined contribution of blue and green electroluminescent emitters of ZnS/Cu phosphor microparticles is responsible for this varying emission color modulated with the excitation frequency<sup>55–57</sup>.

### Mechanical stretchability

Light-emitting drawing displays are made entirely of compliant material components to achieve skin-like deformability. In Fig. 4a, a representative device displaying an “ACEL” pattern is subjected to uniaxial tensile deformations. The uniform emission intensity suggests homogeneous electric fields under highly deformed states. No interfacial delamination signature is identified within 200% strain to confirm the robust construction of the device. The emission has a stable color regardless of tensile deformations, as confirmed with chromatic coordinates in Supplementary Fig. 4b and peak wavelengths in Supplementary Fig. 4c. According to Supplementary Video 2, the dynamic deformation process shows the elongation of the luminous pattern along the stretching direction. In Fig. 4b, the normalized luminance monotonically increases with the tensile strain. The

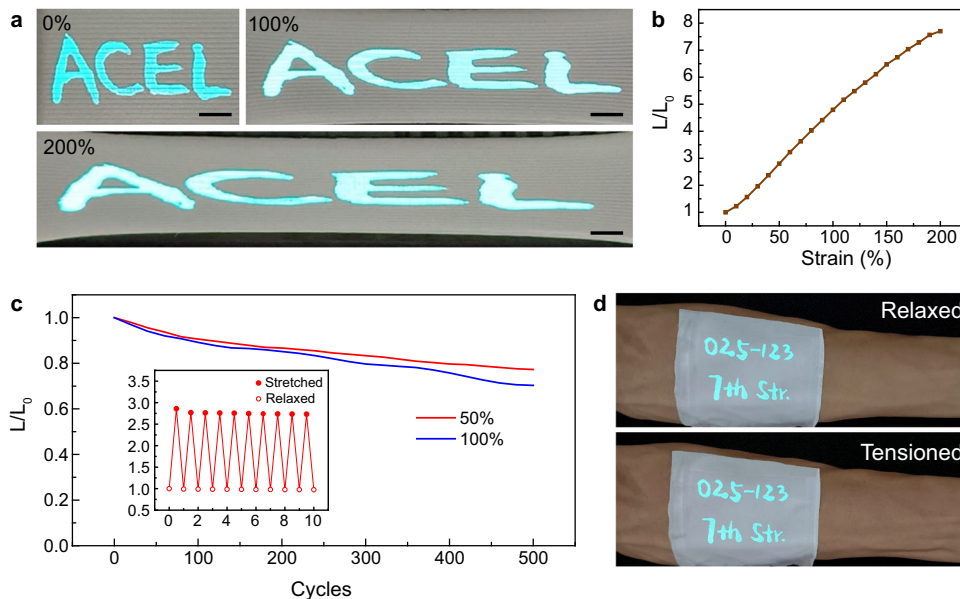
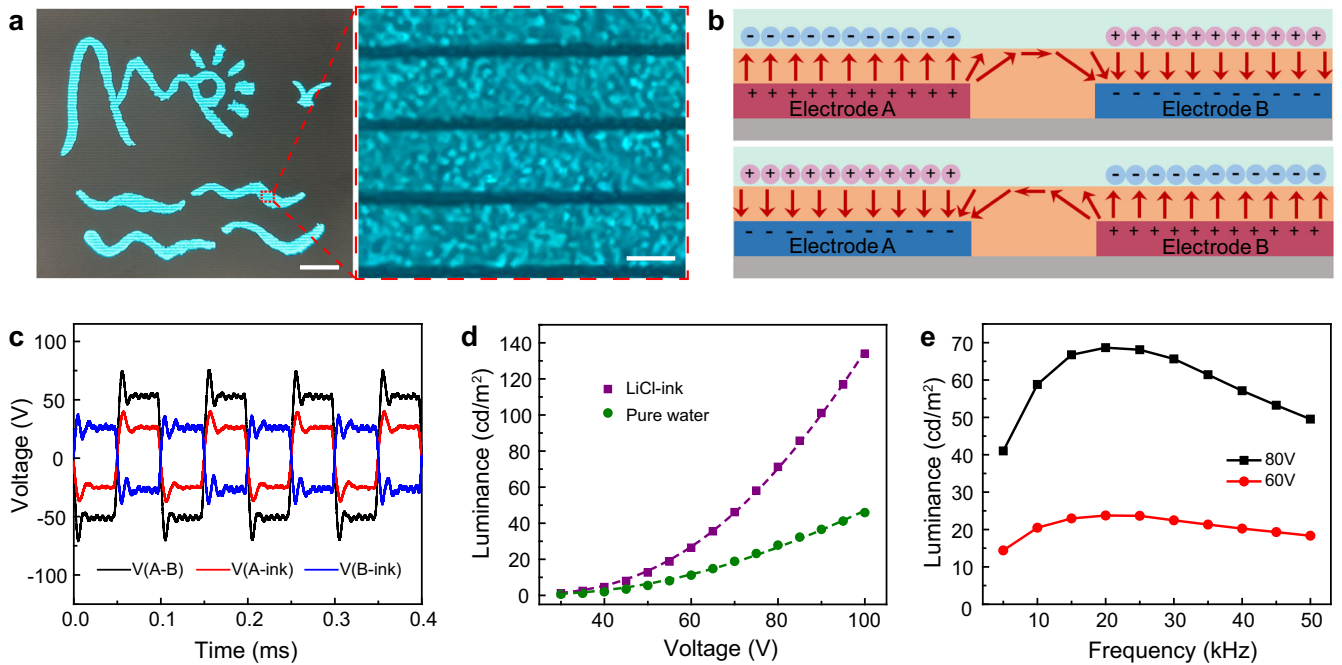


**Fig. 4** Mechanical stretchability of the light-emitting drawing display. **a** Optical images showing a device displaying an "ACEL" pattern under uniaxial tensile deformations. Scale bars: 5 mm. **b** Normalized luminance as a function of the tensile strain. **c** Change in the luminance at relaxed states over 500 stretch-relaxation cycles to 50% and 100% strains. Inset: Normalized luminance at relaxed and stretched (50% strain) states for the initial 10 cycles. **d** Optical images of a stretchable light-emitting drawing display attached to the forearm.

luminous pattern area undergoes significant expansions and reaches  $\sim 1.75$  times its initial value at 200% strain (see Supplementary Fig. 5). Due to the volume conservation, the thickness of the electroluminescent composite reduces to  $\sim 57\%$ , resulting in a notable increase in capacitance<sup>12</sup>. Accordingly, the electric field is enhanced during stretching to raise the emission intensity<sup>12,58</sup>. In addition, the device is further evaluated through fatigue tests involving 500 stretch-relaxation cycles to different

strains. In Fig. 4c, the normalized luminance at the relaxed state is plotted against the cycle number. The final normalized luminance is retained at  $\sim 80\%$  for 50% strain cycles and  $\sim 70\%$  for 100% strain cycles. Stretchable light-emitting drawing displays are sufficiently durable to withstand repetitive deformations. The variations of the relative luminance during the initial 10 stretch-relaxation cycles to 50% strain are shown in the inset of Fig. 4c. The luminescent intensity shows notable increases

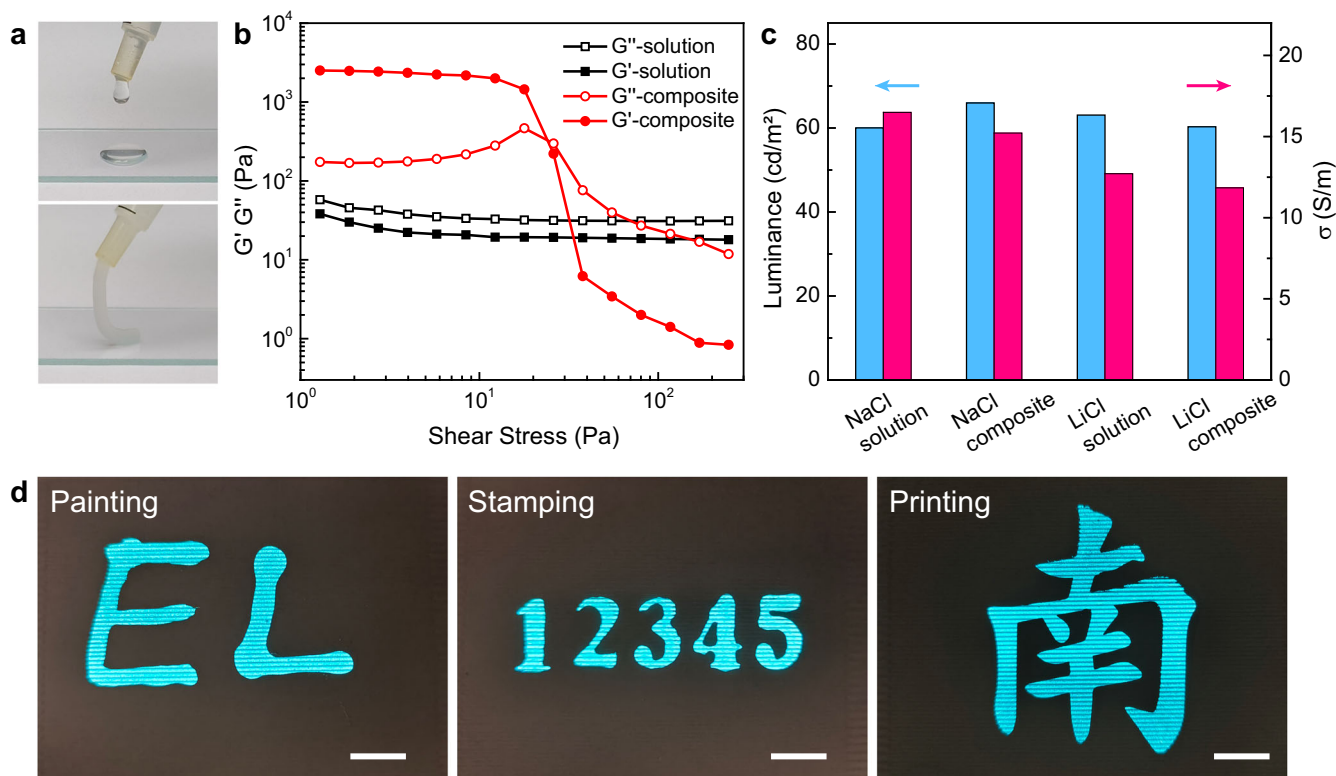


**Fig. 5 Ink formulations for different patterning approaches.** **a** Optical images revealing LiCl-based solution (top) and nanocomposite (bottom) inks extruded from a syringe. **b** Storage moduli ( $G'$ ) and loss moduli ( $G''$ ) as a function of shear stress. **c** Device luminance and ionic conductivity of different inks. The devices are powered by square wave voltages (20 kHz, 80 V). **d** Luminous patterns generated by painting with aqueous solutions (left) and by stamping (middle) and stencil printing (right) with nanocomposite inks. Scale bars: 1 cm.

upon stretching due to enhanced electric fields by thinning the electroluminescent composite. The emission then recovers to the original value after releasing the strain. In Fig. 4d, the soft and stretchy light-emitting drawing device is attached to the skin as a wearable display. The device deforms conformally along with the relaxation and tension of the muscle. These results demonstrate considerable deformability and durability of the light-emitting drawing display for practical applications.

### Ink preparation and patterning approach

Ink patterning approaches depend on their flow properties. A highly flowable aqueous solution generates droplets by squeezing it out from a fine needle (Fig. 5a). Additional silica nanoparticles result in the solid gel appearance under static conditions due to the formation of a three-dimensional nanoparticle network<sup>59,60</sup>. The metastable nanoparticle network is easily disrupted with shear stress, which enables the transition into the liquid state. The behavior allows the ink to be stably extruded into continuous filaments (Fig. 5a). Ink characteristics are measured with a stress-controlled rheometer. In Supplementary Fig. 6, the aqueous solution has a low viscosity of  $\sim 3$  Pa.s independent of the shear rate. The separated moduli curves show its liquid characteristic suitable for painting (Fig. 5b). In comparison, the nanocomposite ink has a high viscosity of  $\sim 300$  Pa.s at  $0.05$  s<sup>-1</sup> shear rate (Supplementary Fig. 6). The viscosity exhibits three orders-of-magnitude reduction by increasing the shear rate to  $200$  s<sup>-1</sup>. A crossover point at  $\sim 25$  Pa in moduli curves suggests the reversible transition between solid and liquid states (Fig. 5b). The nanocomposite ink behaves like a low-viscosity liquid during mechanical manipulation with high shear stresses, followed by rapid transformation back into solid gel states for long-term shape

retention<sup>61</sup>. The flow characteristics are well-suited for stamping and stencil printing.

Nanocomposite inks inherit the high optical transmittance of aqueous solutions, which ensures excellent light extraction (see Supplementary Fig. 7). In Fig. 5c, the aqueous solutions exhibit high conductivity with abundant dissociated ions. The incorporated silica nanoparticles lead to minor conductivity changes due to their phase separation from the electrolyte<sup>60,62</sup>. All inks show high ionic conductivity above  $10$  S m<sup>-1</sup>. Due to their excellent polarizability, light emission intensity is negligibly affected by the ink choice. Luminous patterns are easily defined through painting, stamping, and stencil printing (Fig. 5d). Light-emitting drawing displays can show arbitrary and complex features for visual information communication.

Ink salt choices also influence the device operation modes. Water loss is a common issue for aqueous inks. In Fig. 6a, the water loss ratio *versus* storage time is measured at  $37$  °C to simulate the skin-attached conditions. The NaCl-based ink continuously evaporates and completely dries out in 30 s. In contrast, the LiCl-based ink stays hydrated with  $\sim 25\%$  water loss. The differences come from varying hydration degrees of the dissolved salts. The strong bonding between  $\text{Li}^+/\text{Cl}^-$  and  $\text{H}_2\text{O}$  pairs generates the energy barrier to suppress water evaporations<sup>63,64</sup>. Water retention capability is correlated with the stability of the luminous pattern. Figure 6b reveals the distinctive behaviors of the device with two inks. Corresponding changes in the light-emitting area are illustrated in Fig. 6c. The luminous pattern is intact without any area loss after 30 min for LiCl-based ink, suggesting the suitability for long-term visual information delivery. Using NaCl-based inks, the luminous area rapidly decreases and fully disappears over 20 s. In Fig. 6d, the transient characteristics support continuous drawing of different luminous

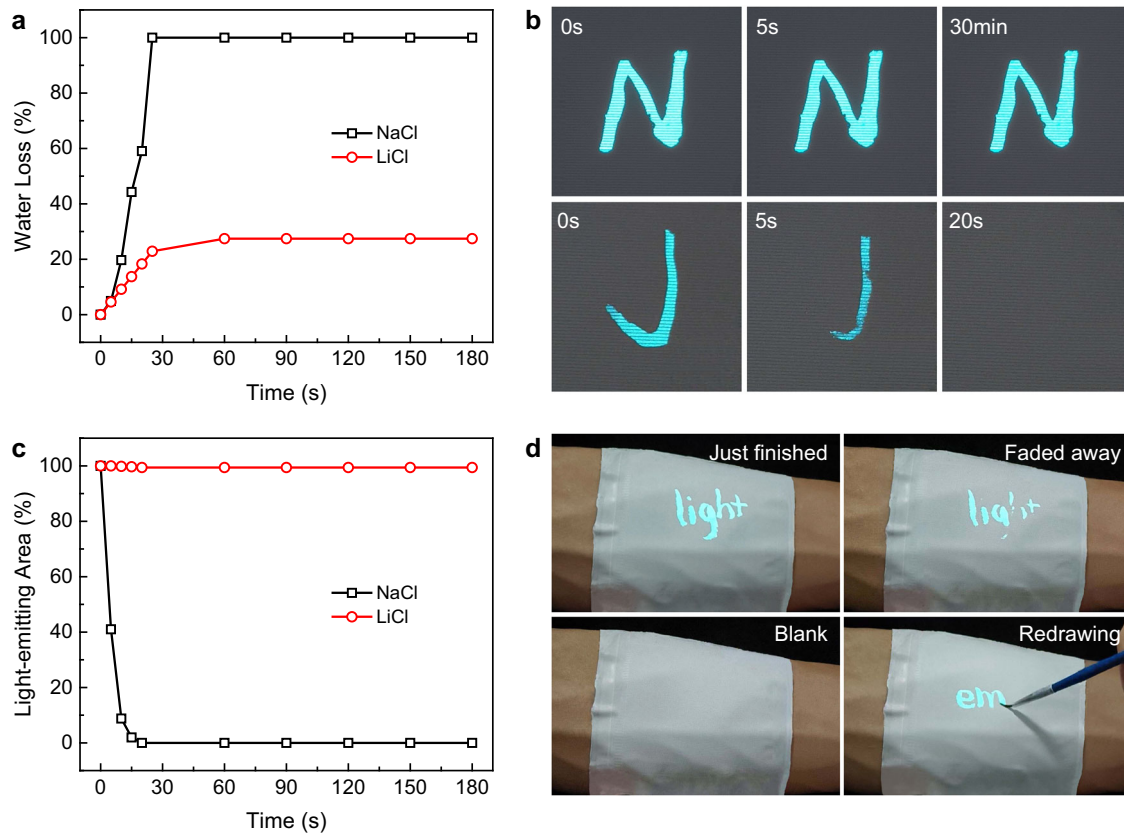


**Fig. 6 Long-lasting and transient operation modes.** **a** Water loss versus storage time at 37 °C for LiCl-based and NaCl-based solution inks. **b** Optical images showing the evolution of painted patterns at 37 °C device using LiCl-based (top) and NaCl-based (bottom) solutions. **c** Light-emitting area as a function of the storage time. **d** Continuous painting of graphic patterns on a stretchable light-emitting drawing display attached to the forearm for real-time communication.

patterns. This operation mode is the enabler of an attractive wearable display for real-time communications.

## DISCUSSION

In conclusion, we have presented the design and material developments of intrinsically stretchable light-emitting drawing displays. The top floating electrode of ionically conductive inks is capacitively coupled with the bottom interdigitated electrodes. The ink pattern defines the luminous feature by modifying the spatial electric field distributions. The inks are formulated with suitable rheological properties for painting, stamping, and stencil printing. Water evaporation of the ink pattern leads to transient emissions for continuous painting, whereas hygroscopic salt suppresses the drying process to enable long-term display. The light-emitting drawing display exhibits high stretchability of up to 200% strain, stable operation under repetitive deformations, and conformal attachment to the skin. These devices offer an appealing operating mode of skin-attached wearable displays to conveniently generate arbitrary and complex luminous patterns for delivering visual information. Looking forward, these displays can potentially function as information communication interfaces on various deformable objects, such as fashioned clothing, interactive lighting systems, and soft robots. Alternatively, the drawing displays may be paired with deformable drivers and batteries for fully untethered wearable systems to further expand the application scopes.

## METHODS

### Materials preparation

All raw materials and chemical reagents were obtained commercially, including hydrogenated styrene–ethylene–butylene–styrene elastomer (SEBS, Tuftec H1221) from Asahi Kasei Corporation, poly(vinylidene fluoride-hexafluoropropylene) (PVDF-HFP, Daiel G801) from Daikin Industries, Ltd., polyethylene oxide (PEO, MW = 300,000) from Shanghai Aladdin Bio-Chem Technology Co., Ltd., BaTiO<sub>3</sub> (BTO) nanoparticles from Shanghai Macklin Biochemical Co., Ltd., fumed silica (AEROSIL 380) from Evonik Degussa GmbH, lithium chloride (LiCl) and sodium chloride (NaCl) from Saan Chemical Technology (Shanghai) Co., Ltd., and fluorinated surfactant (FC-4430) from 3 M Inc. ZnS phosphor microparticles from Shanghai Keyan Phosphor Technology Co., Ltd. contained different types and concentrations of transition-metal dopants (Cu for green and blue; Mn for orange). All organic solvents were provided by Shanghai Macklin Biochemical Co., Ltd. In a nitrogen glovebox, the liquid metal was prepared by alloying high-purity Ga (99.99%), In (99.99%), and Sn (99.999%) at 75 °C for 2 h according to a weight ratio of 68.5:21.5:10. The high-k nanocomposite was prepared by filling BTO nanoparticles into PVDF-HFP solution in MIBK (methyl isobutyl ketone) following a solid ratio of 30 v/v %. The electroluminescent composite was generated by incorporating ZnS phosphor microparticles into the high-k nanocomposite, achieving a weight ratio of 2:1 between the phosphor microparticles and the PVDF-HFP elastomer. All liquid mixtures were homogenized in a YXQM planetary ball mill from Changsha MITR Co., Ltd.

## Device fabrication

SEBS pellets were dissolved in toluene at 20 w/v % and then cast onto an octadecyltrichlorosilane (OTS)-modified glass wafer. After natural evaporation for ~24 h, stretchable substrates were obtained by further heating at 90 °C for 2 h to thoroughly remove the solvents. A Cr/Cu film (10 nm/100 nm) was deposited using a ZHD400 thermal evaporator from Beijing Technol Science Co., Ltd. The substrate holder was actively circulated with the coolant during deposition to reduce the thermal strain on the deposited film. Inside a 4 w/v % hydrochloric acid solution, the liquid metal was drop cast and naturally spread onto the metalized substrate. A uniform liquid metal film of ~1.6 μm was obtained by rotating the sample at 2000 rpm for 60 s in a spin coater. The as-prepared liquid metal film was subtractively patterned into interdigitated electrodes with ~600 μm fingers and ~150 μm gaps by selective laser ablation using a 1064 nm laser marking system (XM-FB30, Xianming Optoelectronic Equipment Co., Ltd.). A single ablation pass (laser power = 0.3 W, scan speed = 1000 mm s<sup>-1</sup>) can completely remove the liquid metal film from undesired regions. A ~10 μm-thick electroluminescent composite layer and then a ~4 μm-thick PVDF-HFP dielectric layer was spin cast on the interdigitated electrodes. In a 2 w/v % aqueous PEO solution, the aqueous solution ink for painting was prepared by dissolving LiCl (10 mol L<sup>-1</sup>) or NaCl (4 mol L<sup>-1</sup>), respectively. The fluorinated surfactant was also added to the inks at 1 w/v % to improve their wettability to the device. Additional fumed silica (10%, w/v) was thoroughly blended into the polymer solutions using a planetary ball mill (YXQM, Changsha MITR Co., Ltd.), generating aqueous nanocomposite inks suitable for stamping and printing.

## Characterization

Optical images and videos were acquired with a Fujifilm X-T10 camera. Microscopy images were captured by a digital optical microscope (VHX-6000, Keyence). SEM images were acquired with a Zeiss GeminiSEM 500 field emission scanning electron microscope. Contact angles were measured using a goniometer (SDC-200, Dongguan Sindin Precision Instrument Co., Ltd.). Rheological properties were characterized with a stress-controlled rheometer (RheoStress 600 HAAKE) using parallel-plate testing fixtures with a fixed gap of 1 mm. A 60 mm fixture was employed for aqueous solutions, whereas a 20 mm fixture was used for aqueous nanocomposites. The frequency was fixed at 1 Hz in dynamic oscillatory shear measurements. The ionic conductivity was measured using an LCR Meter (LCR-6300, GW Instek). The capacitance and dielectric constants of elastomers were measured with parallel-plate capacitor structures by the LCR Meter. Optical transmittance/emission spectra were acquired by a fiber optical spectrometer (PG2000-Pro, IdeoOptics) equipped with integrating spheres (IS-30-6-R, IdeoOptics or IC50-T, Wyoptics). A function generator (AFG-2500, GW Instek) was coupled with a high-voltage amplifier (10/10B-HS, Trek) to power the devices. An oscilloscope (DSOX2024A, Keysight) was employed to record the voltages. The emission intensity and chromatic coordinates were measured using a luminance and color meter (CS-150, Konica Minolta). Stretching tests were carried out on a homemade motorized linear translation stage.

## DATA AVAILABILITY

All data needed to evaluate the conclusions in the paper are present in the paper and/or the Supplementary Materials. Additional data related to this paper may be requested from the authors.

## REFERENCES

- Rogers, J. A., Someya, T. & Huang, Y. Materials and mechanics for stretchable electronics. *Science* **327**, 1603–1607 (2010).
- Choi, S., Lee, H., Ghaffari, R., Hyeon, T. & Kim, D. H. Recent advances in flexible and stretchable bio-electronic devices integrated with nanomaterials. *Adv. Mater.* **28**, 4203–4218 (2016).
- Hua, Q. et al. Skin-inspired highly stretchable and conformable matrix networks for multifunctional sensing. *Nat. Commun.* **9**, 244 (2018).
- Matsuhisa, N., Chen, X., Bao, Z. & Someya, T. Materials and structural designs of stretchable conductors. *Chem. Soc. Rev.* **48**, 2946–2966 (2019).
- Kim, D. C., Shim, H. J., Lee, W., Koo, J. H. & Kim, D. H. Material-based approaches for the fabrication of stretchable electronics. *Adv. Mater.* **32**, e1902743 (2020).
- Kim, D. W., Kong, M. & Jeong, U. Interface design for stretchable electronic devices. *Adv. Sci.* **8**, 2004170 (2021).
- Yin, H., Zhu, Y., Youssef, K., Yu, Z. & Pei, Q. Structures and materials in stretchable electroluminescent devices. *Adv. Mater.* **34**, e2106184 (2022).
- Son, D. et al. An integrated self-healable electronic skin system fabricated via dynamic reconstruction of a nanostructured conducting network. *Nat. Nanotechnol.* **13**, 1057–1065 (2018).
- Kim, E. H. et al. Interactive skin display with epidermal stimuli electrode. *Adv. Sci.* **6**, 1802351 (2019).
- Zhang, Y. et al. Dual-mode electronic skin with integrated tactile sensing and visualized injury warning. *ACS Appl. Mater. Interfaces* **9**, 37493–37500 (2017).
- Lee, Y. et al. Standalone real-time health monitoring patch based on a stretchable organic optoelectronic system. *Sci. Adv.* **7**, eabg9180 (2021).
- Larson, C. et al. Highly stretchable electroluminescent skin for optical signaling and tactile sensing. *Science* **351**, 1071–1074 (2016).
- Tan, Y. J. et al. A transparent, self-healing and high-kappa dielectric for low-field-emission stretchable optoelectronics. *Nat. Mater.* **19**, 182–188 (2020).
- Ma, F. et al. Fully printed, large-size alternating current electroluminescent device on fabric for wearable textile display. *ACS Appl. Electron. Mater.* **3**, 1747–1757 (2021).
- Mi, H. et al. Electroluminescent fabric woven by ultrastretchable fibers for arbitrarily controllable pattern display. *ACS Appl. Mater. Interfaces* **13**, 11260–11267 (2021).
- Jang, B. et al. Auxetic meta-display: stretchable display without image distortion. *Adv. Funct. Mater.* **32**, 2113299 (2022).
- Lee, Y. K. et al. Computational wrapping: a universal method to wrap 3D-curved surfaces with nonstretchable materials for conformal devices. *Sci. Adv.* **6**, eaax6212 (2020).
- Park, S. I. et al. Printed assemblies of inorganic light-emitting diodes for deformable and semitransparent displays. *Science* **325**, 977–981 (2009).
- Sekitani, T. et al. Stretchable active-matrix organic light-emitting diode display using printable elastic conductors. *Nat. Mater.* **8**, 494–499 (2009).
- Kim, T. H. et al. Fully stretchable optoelectronic sensors based on colloidal quantum dots for sensing photoplethysmographic signals. *ACS Nano* **11**, 5992–6003 (2017).
- Li, Y. F. et al. Stretchable organometal-halide-perovskite quantum-dot light-emitting diodes. *Adv. Mater.* **31**, e1807516 (2019).
- White, M. S. et al. Ultrathin, highly flexible and stretchable PLEDs. *Nat. Photonics* **7**, 811–816 (2013).
- Kim, J. H. & Park, J. W. Intrinsically stretchable organic light-emitting diodes. *Sci. Adv.* **7**, eabd9715 (2021).
- Jiang, Y. et al. Topological supramolecular network enabled high-conductivity, stretchable organic bioelectronics. *Science* **375**, 1411–1417 (2022).
- Bade, S. G. R. et al. Stretchable light-emitting diodes with organometal-halide-perovskite-polymer composite emitters. *Adv. Mater.* **29**, e1607053 (2017).
- Filiatrault, H. L., Porteous, G. C., Carmichael, R. S., Davidson, G. J. & Carmichael, T. B. Stretchable light-emitting electrochemical cells using an elastomeric emissive material. *Adv. Mater.* **24**, 2673–2678 (2012).
- Liang, J., Li, L., Niu, X., Yu, Z. & Pei, Q. Elastomeric polymer light-emitting devices and displays. *Nat. Photonics* **7**, 817–824 (2013).
- Wang, J., Yan, C., Chee, K. J. & Lee, P. S. Highly stretchable and self-deformable alternating current electroluminescent devices. *Adv. Mater.* **27**, 2876–2882 (2015).
- Zhou, Y. et al. Bright stretchable electroluminescent devices based on silver nanowire electrodes and high-k thermoplastic elastomers. *ACS Appl. Mater. Interfaces* **10**, 44760–44767 (2018).
- Wang, J. & Lee, P. S. Progress and prospects in stretchable electroluminescent devices. *Nanophotonics* **6**, 435–451 (2017).

31. Yoo, J., Li, S., Kim, D. H., Yang, J. & Choi, M. K. Materials and design strategies for stretchable electroluminescent devices. *Nanoscale Horiz.* **7**, 801–821 (2022).
32. Dinh Xuan, H. et al. Super stretchable and durable electroluminescent devices based on double-network ionogels. *Adv. Mater.* **33**, e2008849 (2021).
33. Chang, Y. et al. Self-powered multi-color display based on stretchable self-healing alternating current electroluminescent devices. *Nano Energy* **95**, 107061 (2022).
34. Go, Y. et al. Optically transparent and mechanically robust ionic hydrogel electrodes for bright electroluminescent devices achieving high stretchability over 1400%. *Adv. Funct. Mater.* **33**, 2215193 (2023).
35. Liu, W. et al. High-efficiency stretchable light-emitting polymers from thermally activated delayed fluorescence. *Nat. Mater.* **22**, 737–745 (2023).
36. Zhang, Z. et al. High-brightness all-polymer stretchable LED with charge-trapping dilution. *Nature* **603**, 624–630 (2022).
37. Stauffer, F. & Tybrandt, K. Bright stretchable alternating current electroluminescent displays based on high permittivity composites. *Adv. Mater.* **28**, 7200–7203 (2016).
38. Zhou, Y. L. et al. Stretchable high-permittivity nanocomposites for epidermal alternating-current electroluminescent displays. *ACS Mater. Lett.* **1**, 511–518 (2019).
39. Zhang, Z. et al. Textile display for electronic and brain-interfaced communications. *Adv. Mater.* **30**, e1800323 (2018).
40. Shi, X. et al. Large-area display textiles integrated with functional systems. *Nature* **591**, 240–245 (2021).
41. Liu, J. et al. Fully stretchable active-matrix organic light-emitting electrochemical cell array. *Nat. Commun.* **11**, 3362 (2020).
42. Li, S., Peele, B. N., Larson, C. M., Zhao, H. & Shepherd, R. F. A stretchable multicolor display and touch interface using photopatterning and transfer printing. *Adv. Mater.* **28**, 9770–9775 (2016).
43. Zhao, C. et al. Fully screen-printed, multicolor, and stretchable electroluminescent displays for epidermal electronics. *ACS Appl. Mater. Interfaces* **12**, 47902–47910 (2020).
44. Joshipura, I. D., Ayers, H. R., Majidi, C. & Dickey, M. D. Methods to pattern liquid metals. *J. Mater. Chem. C* **3**, 3834–3841 (2015).
45. Dickey, M. D. Stretchable and soft electronics using liquid metals. *Adv. Mater.* **29**, e1606425 (2017).
46. Wang, Q., Yu, Y. & Liu, J. Preparations, characteristics and applications of the functional liquid metal materials. *Adv. Eng. Mater.* **20**, 1700781 (2018).
47. Xu, X. et al. Polar-electrode-bridged electroluminescent displays: 2D sensors remotely communicating optically. *Adv. Mater.* **29**, 1703552 (2017).
48. Zhang, J. et al. An ultrastretchable reflective electrode based on a liquid metal film for deformable optoelectronics. *ACS Mater. Lett.* **3**, 1104–1111 (2021).
49. Steinberger, I. T., Bar, V. & Alexander, E. Electroluminescence of zinc sulfide single crystals. *Phys. Rev.* **121**, 118–124 (1961).
50. Manzoor, K., Vadera, S. R., Kumar, N. & Kutty, T. R. N. Multicolor electroluminescent devices using doped ZnS nanocrystals. *Appl. Phys. Lett.* **84**, 284–286 (2004).
51. Tanaka, S., Kobayashi, H., Sasakura, H. & Hamakawa, Y. Evidence for the direct impact excitation of Mn centers in electroluminescent ZnS:Mn films. *J. Appl. Phys.* **47**, 5391–5393 (1976).
52. Yang, H., Holloway, P. H. & Ratna, B. B. Photoluminescent and electroluminescent properties of Mn-doped ZnS nanocrystals. *J. Appl. Phys.* **93**, 586–592 (2003).
53. Tripathi, L. N., Chaubey, B. R. & Mishra, C. P. Photo and electroluminescence properties in ZnS: (Cu, La) and ZnS: (Ag, La) phosphors. *Pramana* **16**, 155–164 (1981).
54. Baur, G., Wengert, R. & Wittwer, V. Optical and thermal depth of shallow traps in ZnS. *Phys. Status Solidi A* **18**, 337–345 (1973).
55. Allieri, B. et al. Spectroscopic characterisation of alternate current electroluminescent devices based on ZnS–Cu. *J. Alloys Compd.* **341**, 79–81 (2002).
56. Ibañez, J., García, E., Gil, L., Mollar, M. & Mari, B. Frequency-dependent light emission and extinction of electroluminescent ZnS:Cu phosphor. *Displays* **28**, 112–117 (2007).
57. Hu, D., Xu, X., Miao, J., Gidron, O. & Meng, H. A stretchable alternating current electroluminescent fiber. *Materials* **11**, 184 (2018).
58. Wang, J. et al. Extremely stretchable electroluminescent devices with ionic conductors. *Adv. Mater.* **28**, 4490–4496 (2016).
59. Kawaguchi, M. Dispersion stabilities and rheological properties of fumed silica suspensions. *J. Dispersion Sci. Technol.* **38**, 642–660 (2016).
60. Lu, Q. et al. A printable and conductive yield-stress fluid as an ultrastretchable transparent conductor. *Research* **2021**, 9874939 (2021).
61. Urieu, N. B. & Ladyzhinsky, I. Y. Fractal models in rheology of colloidal gels. *Colloids Surf. A* **108**, 1–11 (1996).
62. Ueno, K., Hata, K., Katakabe, T., Kondoh, M. & Watanabe, M. Nanocomposite ion gels based on silica nanoparticles and an ionic liquid: ionic transport, viscoelastic properties, and microstructure. *J. Phys. Chem. B* **112**, 9013–9019 (2008).
63. Stokes, R. H. & Robinson, R. A. Ionic hydration and activity in electrolyte solutions. *J. Am. Chem. Soc.* **70**, 1870–1878 (1948).
64. Bai, Y. et al. Transparent hydrogel with enhanced water retention capacity by introducing highly hydratable salt. *Appl. Phys. Lett.* **105**, 151903 (2014).

## ACKNOWLEDGEMENTS

This work was supported by the National Natural Science Foundation of China (Grant Nos. 62374083, 52250363, and 22173046), and the State Key Laboratory of Analytical Chemistry for Life Science (Grant No. 5431ZZXM2205).

## AUTHOR CONTRIBUTIONS

D.K. and M.L. conceived the experiments. J.Z. carried out material preparations, device fabrications, and characterizations. M.W., Q.L. and X.W. performed rheological measurements and analyses. Y.S. and S.W. participated in the device characterizations. J.Z. and D.K. wrote the original manuscript. All authors contributed to the scientific planning and discussions.

## COMPETING INTERESTS

The authors declare no competing interests.

## ADDITIONAL INFORMATION

**Supplementary information** The online version contains supplementary material available at <https://doi.org/10.1038/s41528-023-00287-8>.

**Correspondence** and requests for materials should be addressed to Xiaoliang Wang, Ming-Hui Lu or Desheng Kong.

**Reprints and permission information** is available at <http://www.nature.com/reprints>

**Publisher's note** Springer Nature remains neutral with regard to jurisdictional claims in published maps and institutional affiliations.



**Open Access** This article is licensed under a Creative Commons Attribution 4.0 International License, which permits use, sharing, adaptation, distribution and reproduction in any medium or format, as long as you give appropriate credit to the original author(s) and the source, provide a link to the Creative Commons license, and indicate if changes were made. The images or other third party material in this article are included in the article's Creative Commons license, unless indicated otherwise in a credit line to the material. If material is not included in the article's Creative Commons license and your intended use is not permitted by statutory regulation or exceeds the permitted use, you will need to obtain permission directly from the copyright holder. To view a copy of this license, visit <http://creativecommons.org/licenses/by/4.0/>.

© The Author(s) 2024